ENVIRONMENTAL SCANNING ELECTRON MICROSCOPY

Gerasimos Daniel Danilatos
ESEM Research Laboratory, Sydney, NSW 2026, Australia

ABSTRACT

Following early works on in-situ transmission electron microscopy by using environmental cells, the environmental scanning electron microscope (ESEM) has formed the counterpart for the examination of specimen surfaces in a gaseous environment at pressures up to one atmosphere. As accelerating voltages are relatively low in ESEM, it has been necessary to establish the optimum electron beam transfer conditions from a high vacuum to a high pressure region by using windowless apertures. Studies on the gas and electron dynamics of the system have determined that it is possible to use tungsten, LaB_6 and field emission guns without compromising the useful probe size in the presence of gas. The backscattered electron, cathodoluminescence and x-ray detection modes are preserved with proper modification of the detectors. A new method for detection of the secondary and backscattered electron signal has been introduced by the use of the ionisation and scintillation of the environmental gas by corresponding signals. Further, the ionised gaseous environment substitutes the conventional conductive coating or treatment techniques necessary for insulators in vacuum SEM. The high pressure also allows a fully or partially moist environment for the examination of biological or wet specimens, or of chemical reactions in the gas/liquid/solid phases. The possibility of examining the natural or true surface of practically any specimen has added a new dimension to electron microscopy. New contrast mechanisms reveal information not previously possible to see. It has greatly facilitated the examination of specimens by eliminating or reducing the specimen preparation procedures and the specimen exchange time. Based on the success of an experimental ESEM, new commercial instruments are now available making this technology accessible to all. Published scientific literature demonstrates that ESEM has been applied to the most diverse disciplines. A future prospect is to integrate and jointly develop the scanning transmission electron microscope towards a universal kind of environmental EM.

INTRODUCTION

Manfred von Ardenne [1,2], in Germany, described the principle, theory and practice of what we presently call scanning electron microscope (SEM) and scanning transmission electron microscope (STEM) in his classic papers entitled *Das Elektronen-Rastermikroskop*. From the outset, he also considered the examination of objects in air by mounting a thin specimen on an electron transparent film, the opposite side of which sealed against the vacuum of the microscope. Shortly afterwards, he published several papers on the possibility of examining living matter [3], on live spores in his *universal electron microscope* [4] and on chemical reactions [5].

Further work on the idea of introducing gas in a conventional transmission electron microscope continued by various groups in several countries. In the Soviet Union, the Stoyanova group [6,7] published a series of papers on the development and use of environmental cells in the electron microscope. In France, the Dupouy group [8] continued with a high voltage electron microscope. In the USA, the Parsons group [9] made further progress in an attempt to examine living organisms in the electron microscope. There have been numerous other workers and laboratories that have published many works on this topic, but it is beyond the scope of this chapter to survey all these works in any detail. Reviews can be found in the literature cited and elsewhere [10].

Five decades after von Ardenne's initial works, the first manufactured *environmental scanning electron microscope (ESEM)* came into existence based on the most recent works by Danilatos [11,12], in Australia. An extensive bibliographical survey on the development and applications of ESEM is presented elsewhere [13]. Theoretical and experimental investigations that enhanced our understanding and introduced new instrument designs, followed by its manufacture, have made this new branch of electron microscopy acceptable and accessible by the international scientific community.

The ESEM has been defined as a SEM that can operate with a specimen chamber pressure from high vacuum up to at least a pressure level that can maintain fully wet specimens, namely, up to 609 Pa (6.09 mbar, or 4.6 Torr) which is the saturation water vapour pressure at 0^{o} C. This definition is consistent with the historical aim of the instrument, namely, to observe liquid water and live specimens. However, in the course of its development, the scope of ESEM has expanded enormously by finding that the presence of gas has two additional advantages: (i) It acts as a charge dissipation medium and (ii) it can be used as a detection medium. Another use of the electron beam in an ESEM is for micro-fabrication processes by choosing the right gas composition in the specimen chamber. The general purpose use of an electron beam in gas has opened a new domain over and above its limited uses in vacuum. A number of ESEM

applications taken from existing works will be shown in the latter part of this chapter.

There are some basic principles and concepts of ESEM that require proper understanding both by the designer and the user of this technology. These relate to the gas dynamics of the system, the electron beam transfer from high vacuum to high pressure and the detection of various signals in a gaseous environment. The manufacturer, in particular, is also faced with the task of integrating all these requirements with new electron optics systems. Only when the total design of the ESEM instrument is optimised, can the operator extract the maximum amount and best quality information from a whole new world of specimens and applications.

GAS DYNAMICS

Although it is not necessarily the only way, the use of small apertures to separate regions of different pressure has been the best way to design an ESEM to date. The use of thin electron transparent films for the same purpose would absorb and spread the useful electron probe very quickly in the low keV range. The latter range is preferred to avoid large beam-specimen interaction volumes for well known reasons. Correct application of free pressure limiting apertures (PLA) that restrict the flow of gas between regions results in minimum electron losses. By using a series of such apertures, it is possible to separate high pressures in the specimen chamber (up to one atmosphere) from the vacua required to run all different electron beam sources (tungsten, LaB_6 and field emission guns). The use of such apertures, together with corresponding pumping between them, is the well known differential pumping method.

A two-stage differential pumping system for an ESEM is shown in figure 1. This is a minimum requirement when tungsten filament is used as the electron source. Additional pumping stages can be incorporated to allow a LaB_6 or field emission gun, all of which have already been successfully incorporated in commercial types of ESEM. The additional stages do not result in additional beam electron losses because the electron mean free

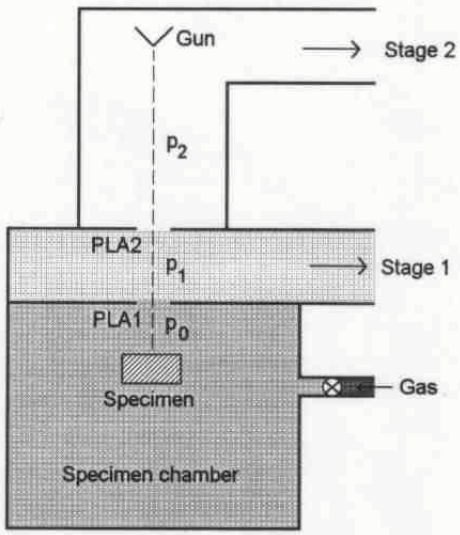

Figure 1. ESEM two-stage differential pumping.

path is much greater than the length of the electron optics column. With the two pressure limiting apertures shown, PLA1 and PLA2, several orders of magnitude pressure differentials can be created between the specimen chamber pressure p_0, the first stage pressure p_1, and the second stage pressure p_2, so that $p_2 << p_1 << p_0$.

The gas leaked through PLA1 is replenished from an outside source via a control leak valve. Because this leak is relatively small, the velocity of the gas in the specimen chamber is practically zero. Thus, the gas pressure can be assumed uniform throughout the specimen chamber (stagnation pressure) provided there are no significant temperature gradients. With condensable gases, such as water vapour, temperature gradients produce significant local variations of relative density (e.g. humidity) and possible condensation.

The transition region between the stagnation pressure in the specimen chamber to the rough vacuum conditions in stage 1 is schematically shown in figure 2. The velocity of the gas flow gradually increases in the upstream direction starting, for practical purposes, from a distance of about one diameter below PLA1; it remains subsonic up to a point located a fraction of a radius above the aperture. Beyond this point, the flow becomes supersonic until the stream gas molecules collide with the background "stagnant" molecules of stage 1, creating a shock wave, the Mach disk. The corresponding density of the gas decreases also from about one diameter below PLA1. The decrease becomes sharp immediately above the aperture and then the density levels off to the background pressure of stage 1. To be precise, the levelling off of density passes through a small depression before it increases again in the region of Mach disk. Beyond the Mach disk, the density may be considered more or less uniform again, for the present purposes. Therefore, in general, we have three pressure zones with pressure p_0, p_t in the transition region and p_1. However, the actual case may incorporate only the first two zones (with p_0 and p_t) when the Mach disk merges with the shock wave formed by the colliding molecules with the surface of PLA2; the latter condition occurs when p_0 is very high, or p_1 very low, or PLA1 very large, or the distance between PLA1 and PLA2 (H) is too short. If the specimen is placed within one diameter from PLA1, the uniform

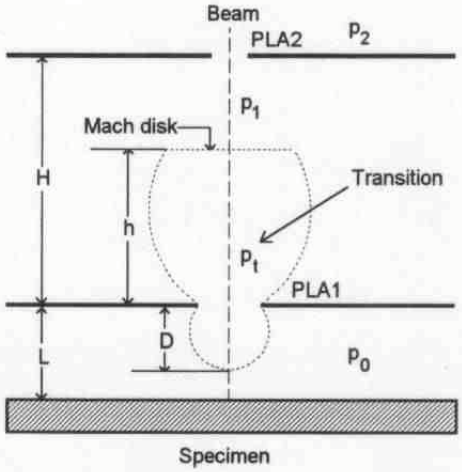

Figure 2. Transition zone of gas density enclosed by dotted line. Definition of geometrical parameters.

(stagnant) zone is practically absent, as streaming occurs too close to the specimen. Usually, this gas streaming does not appear to affect the specimen surface properties, but there may be some applications for which some caution is justified.

The precise flow properties depend on the initial conditions of the gas in the specimen chamber, on the nature of gas and, most importantly, on the geometry of the system. The determination of density gradients and other flow properties in the transition region has been most difficult to treat. The equations of continuum gas dynamics are not applicable, because the flow usually varies between molecular and continuum regimes for most operational conditions in ESEM. The problem is further aggravated by the geometry of PLA1 with a sharp edge required to produce the most abrupt transition.

The need to study the flow properties around the PLA1 has been addressed by Danilatos [14]. The direct simulation Monte Carlo (DSMC) method developed by Bird [15] for gaseous flows has been used for such studies with success. This method allows the determination of the flow field around various shapes of PLA1, various configurations between specimen and aperture, and other geometries. A large amount of information for many gaseous flows in ESEM has been accumulated over many years but this constitutes a separate topic in its own right. One particular case is shown in figure 3 with a conical shape aperture and a flat specimen placed one diameter below the aperture ($D=400\ \mu m$). The iso-density contours of the field are drawn only on a semi-plane defined by the aperture axis, because the flow is axially symmetric. A depletion zone is formed below the aperture. For electron scattering purposes, the density in the gas jet above the aperture remains significant up to a certain point.

We find that the effects of flow on the specimen surface are small when we calculate the pressure on the surface. The pressure decreases only by about 4% below the stagnation value of $p_0=1000$ Pa which corresponds to $n_0=2.47E+23$ particles/m^3. The decrease takes place directly under the area of the aperture. The variation of number density n in terms of normalised number density n/n_0, along the axis

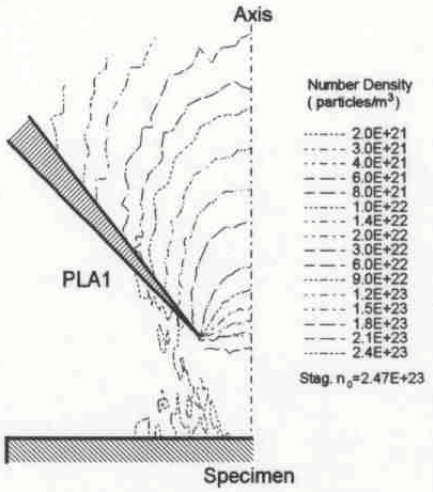

Figure 3. Semi-plane of number density contours for argon. Gas flows through sharp tip PLA1 ($D=400\ \mu m$) with flat specimen placed one diameter below aperture. Contour values decrease in the direction of the flow.

of the aperture in terms of normalised distance z/D, is shown in figure 4. From this type of information, we can calculate the mass thickness of gas through which the electron beam passes. The definite integral:

$$\zeta = \int_{z}^{h} \frac{n(z)}{n_0} \frac{dz}{D} \tag{1}$$

gives the normalised number thickness ζ of a gas layer along the axis from a point z up to a maximum distance h above the aperture, for which data is available and at which the pressure has decreased to a sufficiently low value. Above this point, scattering should not be significant for a properly designed instrument, but the number thickness can be directly calculated from the uniform background pressure p_1 prevailing at this stage and the difference in distance, i.e. H-h (per figure 2). Similarly, the number thickness can be found from the constant pressure for any gas layer thickness below one diameter from PLA1, i.e. L-D. Therefore, we need first to plot the numerical evaluation of the normalised mass thickness vs. z/D in the transition region from $z=-1D$ up to a fixed value of, say, $z=h=3D$ as shown in figure 5 (we have used the approximation of $\zeta=0$ for $z>h$) . We note that $\zeta=0.48$ for the mass of gas above the plane of the aperture with a 40^0 inside cone angle; this is a little above the value of 0.40 found in the case of a flat aperture. The conical shape of aperture is preferred because it allows better specimen movement (such as tilt) and ventilation, better positioning of scintillating detectors and better efficiency in the detection of pure secondary electrons (SE) with the gaseous detection device (to be discussed later). At the specimen surface ($z=-1D$), we find $\zeta=1.4$ and, therefore, the mass thickness above the aperture alone represents about 34% of the total amount. The significance of these numbers in

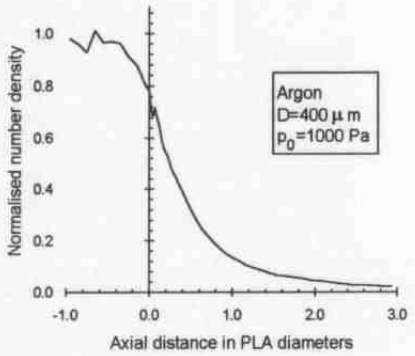

Figure 4. Variation of normalised number density along the axis of PLA1 for argon at 1000 Pa specimen chamber pressure.

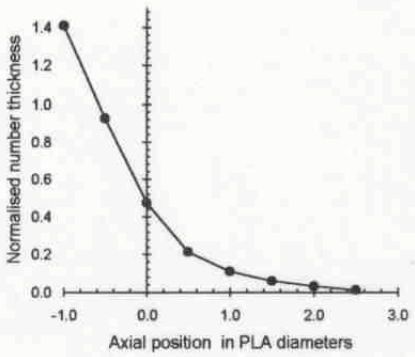

Figure 5. Normalised number thickness for layer h-z along PLA1 axis by integrating the curve of previous figure.

absolute terms will become apparent as we examine the electron beam scattering below. The values of ζ are applicable to all mechanically similar flow fields, e.g. we can vary p_0 and D but keep their product p_0D constant. For practical purposes, a small deviation from the constancy of this product can be allowed, e.g. we can keep the aperture constant and vary the pressure from a few mbar to about 20 mbar. Outside this range, the effects of the transition from free molecule flow to continuum flow start becoming apparent.

ELECTRON BEAM TRANSFER

The equations governing the electron beam transfer from high vacuum to high pressure are given below. Significant electron losses start in the region between PLA1 and PLA2 but the highest losses usually take place in the specimen chamber. The total electron beam path should be traversed with minimum electron beam losses in a properly designed and operated ESEM.

The electron beam scattering process in the gas is governed by the Poisson distribution probability function, which gives the probability for an electron to undergo x number of collisions:

$$P(x) = \frac{m^x e^{-m}}{x!} \tag{2}$$

This means that for each electron there is a probability with which it may undergo no scattering, single scattering, double scattering event, etc. If the average number of scattering events per electron is m, then there is a fraction of electron beam I/I_0 that is transmitted without any scattering at all, the intensity of which decreases exponentially with m:

$$\frac{I}{I_0} = e^{-m} \equiv q \tag{3}$$

The parameter m is generally given by:

$$m = \sigma_T \int n(z)dz \tag{4}$$

where σ_T is the total scattering cross-section for the gas. When the beam passes through the three pressure zones outlined in figure 2, we have three corresponding terms for m:

$$m = m_0 + m_t + m_1 \tag{5}$$

from which:

$$m = \sigma_T n_0 (L - D) + \sigma_T \int_{-D}^{h} n(z)dz + \sigma_T n_1 (H - h) \tag{6}$$

The first and third terms are calculated directly, while the middle term requires knowledge of the density variation along the transition region. Using equation (1), we can calculate the number of electron collisions in the transition region by:

$$m_t = \sigma_T n_0 D \int_{-D}^{h} \frac{n(z)}{n_0} \frac{dz}{D} = \sigma_T n_0 D \zeta \tag{7}$$

The number density is proportional to the specimen chamber pressure in an ideal gas:

$$n_0 = \frac{p_0}{kT_0} \tag{8}$$

where k is the Boltzmann's constant and T_0 the absolute temperature. By substitution, we finally obtain:

$$m = \frac{\sigma_T}{kT_0}\left[p_0(L - D) + p_0 D\zeta + p_1(H - h)\right] \quad \text{with } L > D \text{ and } H > h \tag{9}$$

The last equation is considered the *general constitutive equation of ESEM*. When the attached conditions are not satisfied, the corresponding terms are omitted. This equation relates the electron scattering characteristics of the gas with its other physical properties (such as pressure, temperature, velocity, etc.), with the working distance, the aperture geometry and the positioning of apertures. It reveals that all these parameters interplay within a wide range of operation. We initially determine the maximum tolerable value of m for which imaging or analysis is satisfactory for a particular application. We should note that for $m=3$, only 5% of the beam survives, and, hence, this has been defined

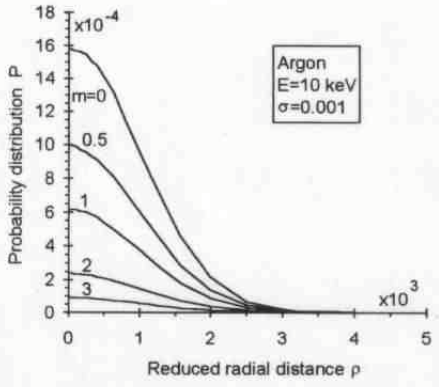

Figure 6. Probability distribution of beam electrons in argon for different values of m (E=accelerating voltage, σ=standard deviation of Gaussian distribution in vacuum).

(arbitrarily) as the maximum value allowed for m. With the condition $m<3$, the case is referred to as an *oligo-scattering* regime which is distinct from the well known *single-*, *plural-*, and *multiple-scattering* regimes [11]. Usually, we prefer $m \leq 1$ which is still an oligo-scattering regime, as opposed to single-scattering where the majority of electrons (say more than 95%) undergo one or no scattering events. When $m=1$, we get 37% of electrons suffering no collisions, 37% suffering a single collision, 18% two collisions, 6% three collisions, etc. Figure 6 demonstrates how the intensity of the useful probe decreases with increasing values of m by plotting the probability distribution of electrons at the specimen surface. The beam in vacuum (i.e. for $m=0$) has a Gaussian distribution, the shape of which essentially remains the same (which can also be confirmed by reading the numerical values of the computation). In this example, the accelerating voltage used is 10 keV and the standard deviation of the Gaussian distribution is 0.001 units of reduced radial distance [11]. With further numerical computations, we confirm that the smaller the probe we use, the less affected is the original distribution of the probe. Thus, the separation of useful probe is best with a field emission gun. The pressure can vary from high vacuum to atmospheric levels as has been found in practice; the other parameters are constrained accordingly.

Equation (9) can be simplified for different working conditions. If we neglect the third term in the brackets, when the pressure p_1 is very low, we obtain:

$$m = \frac{\sigma_T p_0}{kT_0}\left[L + (\zeta - 1)D\right] \quad \text{with } L > D \tag{10}$$

When the specimen distance is much greater than the diameter of PLA1, we can further simplify the above expression to:

$$m = \frac{\sigma_T p_0 L}{kT_0} \quad \text{with } L >> D \tag{11}$$

which is the familiar inverse relationship between pressure and distance. When and only when $m << 1$ (e.g. $m<0.2$), equation (3) finally reduces to a linear relationship with respect to the product p_0L, by using equation (11):

$$I = I_0\left(1 - \frac{\sigma_T p_0 L}{kT_0}\right) \quad \text{with } L >> D \text{ and } m << 1 \tag{12}$$

After analysing the unscattered fraction, we examine the relations of the other, equally important, fraction of the scattered beam. A first approximation is to consider the single-scattering regime, but the complete treatment involves the oligo-scattering regime. Unfortunately, there is no simple analytical formula

describing this fraction which forms a very broad "skirt" surrounding the intact probe at the centre. The analytical expressions by Jost and Kessler [16, 11] have been used to compute the electron distribution for various gaseous conditions in ESEM. One parameter we need to know is the extent over which the scattered electrons are distributed. One measure of it is the "half width radius" $r_{0.5}$, which is the radius containing half of the total scattered electrons. From computed profiles, two empirical equations are given below for argon and helium at 10 keV and $T_0=293$ K [11]:

$$\text{Argon:}\quad r_{0.5} = 0.0096L + 0.0169L(pL)^{1.78} \tag{13}$$

$$\text{Helium:}\quad r_{0.5} = 0.0027L + 0.00014L(pL)^{1.27} \tag{14}$$

Approximate equations for nitrogen have been found for radii containing 50% and 90% of skirt electrons assuming single-scattering [17]:

$$\text{Nitrogen:}\quad r_{0.5} = \frac{0.354L + 2.174\times 10^{19}\,\sigma_T p_0 L}{\left(E + 9.778\times 10^{-7}E^2\right)^{1/2}} \tag{15}$$

$$\text{Nitrogen:}\quad r_{0.9} = \frac{4.128L + 1.503\times 10^{20}\,\sigma_T p_0 L}{\left(E + 9.778\times 10^{-7}E^2\right)^{1/2}} \tag{16}$$

Two typical values of cross-section for nitrogen can be taken to be $\sigma_T=2.18\times10^{-21}$ m^2 at $E=30000$ eV and $\sigma_T=5.7\times10^{-21}$ m^2 at $E=10000$ eV All variables are in SI units except for the beam energy E which is expressed in eV. Equations (13), (14), (15) and (16) refer to a step function of gas pressure variation (i.e. to an abrupt transition from vacuum to p_0) which, in practice, is taken to be the case when $L>>D$. Monte Carlo simulations may be computed, but precise experimental skirt distributions should be obtained in future work with well calibrated instruments. It is interesting to note that the skirt radius does not vanish as the pressure approaches the zero limit; it is rather the intensity of the skirt that vanishes. This is because the average scattering angle for a given molecule has a finite value which is independent of gas pressure. Thus, the finite minimum skirt radius occurs in the single-scattering regime (as $m \to 0$); as we progress in the oligo-scattering region both the intensity and the radius of the skirt increase monotonically.

All above equations are important, because they describe the operational conditions frequently encountered in ESEM. They can be used in a computerised system for optimum specimen positioning and optimum detector operation. In particular, they can be used for initially calibrating out the skirt effect in x-ray analysis, for which more precise relationships can be determined in the future.

CONTRAST AND RESOLUTION

From the preceding analysis of the electron beam transfer under oligo-scattering conditions, we conclude these main points: A useful probe survives intact as it reaches the specimen surface. It is this surviving (unscattered) spot that is used to create an image. The spatial distribution of electrons in the spot is the same as the original distribution in vacuum, because the removal of scattered electrons from the original spot occurs with the same probability. The scattered electrons strike the specimen away from the useful spot at a distance being orders of magnitude greater than the useful spot. Their broad distribution has a relatively low intensity contributing only to a background featureless noise.

The resolution of a particular feature on a specimen having sufficient contrast is ultimately determined by the electron probe size provided we employ detectors with maximum efficiency. Therefore, the ultimate resolving power of an ESEM is determined by the particular electron optics used, whilst the presence of gas is a secondary influence. This has been shown both theoretically and experimentally [11]. Figure 7 shows a resolution test specimen in the gaseous environment of an ESEM with no loss of resolution as compared with vacuum conditions.

However, the decrease of intensity of the useful probe in gas results in a loss of contrast. Depending on the particular specimen, the relative loss of contrast may result in loss of satisfactory definition of a feature. For a weak feature, the loss of contrast (due to gas) can usually be recovered by an electron-optical increase of the probe current, which is normally accompanied by a greater probe diameter. The probe size increase depends on the electron optics used and not on a presumed broadening of the useful probe by the gas layer (e.g. like the "top-bottom" effect in STEM specimens). Fortunately, the electron-optical loss of resolution, when it occurs, can be generally outweighed in practice by other benefits in ESEM, such as the rise of new contrasts on the natural surface of specimens. The conventional metallisation of insulating surfaces in vacuum results only in increased topographical contrast; however, material contrast is diminished or masked. Also, surface charge of uncoated surfaces makes it impossible, or difficult to image, or alters the natural features of a specimen. The advent of ESEM

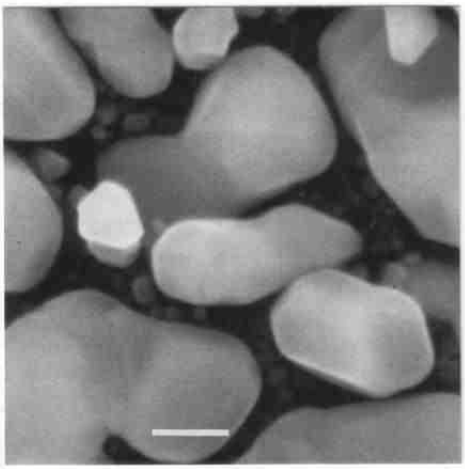

Figure 7. SE image of gold-on-carbon under 10 mbar of water vapour pressure with 30 keV beam (magnification bar=200 nm).

frees the specimen surface from such impediments, while it reveals new contrasts not previously seen. Also, the advent of new more efficient detection means in the presence of gas has overcompensated any electron-optical loss of resolution. After all, the beam damage on some specimens may become the limiting factor of resolution, before we can reach the maximum magnification specified by an instrument. For all these reasons, ESEM necessitates the employment of the best electron optics technology, if we wish to take full advantage of this new electron microscopy. It is with such provisos that we may generally state that the resolution of ESEM is the same as that of SEM, as has been shown in practice.

We have established a quantitative guide of the way contrast varies by the presence of gas. With a beam current I_0 and pixel dwell time τ, we get n_{e0} electrons striking the specimen at each pixel element, when the specimen chamber is in vacuum. With a signal-to-noise-ratio K and with M gray levels on the recorded micrograph, we get the following relationship [18]:

$$I_0 = \frac{K^2 M^2 e}{4\tau}\left(\frac{\sqrt{\delta_A + \delta_B} + \sqrt{\delta_B}}{\delta_A}\right)^2 \tag{17}$$

where e is the electron charge, δ_A the fraction of the electron beam converted to useful signal (or feature) after the beam-specimen interaction, and δ_B is the fraction converted to background noise. The introduction of gas modifies the above equation to the following one [11]:

$$I_0 = \frac{K^2 M^2 e}{4\tau}\left(\frac{\sqrt{\delta_A + \delta_B + \delta_0} + \sqrt{(1-q)\delta_A + \delta_B + \delta_0}}{q\delta_A}\right)^2 \tag{18}$$

where δ_0 represents the ionisation electrons in the gas generated by the beam before the beam strikes the specimen; this constitutes the first of three terms adding to the background noise level. The second term is simply $q\delta_B$ from the useful spot. The third term is generated from the skirt fraction $(1-q)\delta_S$ of electrons striking the specimen. The primary electrons back-scattered from the gas can be neglected because they constitute an extremely small fraction under the oligo-scattering condition. For the skirt electrons striking the specimen, the conversion coefficient δ_S depends on the precise specimen nature, the magnification used and the extent of the skirt. The conservative value of $\delta_S = \delta_A + \delta_B$ is used for the derivation of equation (18), but this can be modified in future work accordingly; the present value is satisfactory for a general purpose analysis of the detection system. The last two terms relate to the specimen nature and, lumped together, are designated as $\delta_{BB} \equiv q\delta_B + (1-q)\delta_S = (1-q)\delta_A + \delta_B$. Further details on this topic for different detection systems are presented elsewhere [19].

DETECTION

The four main types of signal emitted from the beam-specimen interaction volume are the secondary electrons (SE), the backscattered electrons (BSE), cathodoluminescence (CL) and x-rays. These signals may be subdivided into smaller fractions carrying specific information, such as various types of SE, low loss BSE and Auger electrons. All four modes of detection have been employed in ESEM, but the full benefit of each mode still remains to be accomplished.

Secondary Electrons

The conventional Everhart-Thornley (E-T) detector used for the SE signal breaks down in the presence of gas. In ESEM, a novel method has been introduced by using the gas itself as a detector. In particular, the products of reaction between various signals and gas are used by this method. This approach has been referred to as gaseous detection device (GDD), because it incorporates a broad family of detection configurations, all of which use the gas as a detection medium. The gas has presented this function and advantage over and above its initial purpose as an environmental medium. The GDD has been used for the detection of various signals including the SE signal. The detection of SE signal, specifically, in a gaseous environment has been of particular importance for the whole development of ESEM. It is the latter achievement that has been used as the basis for the first manufactured ESEM.

The detection of SE has been achieved by the use of either the ionisation or the scintillation products created by the SE emanating from the specimen surface as they move through the gas [20,21,22]. The principle of GDD can be

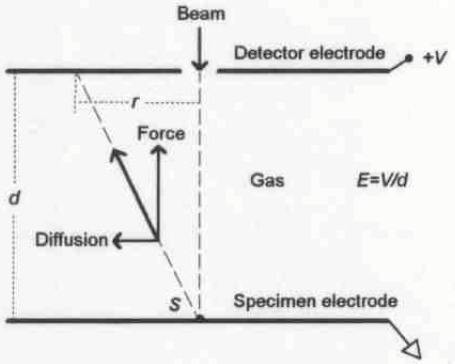

Figure 8. Electron beam generates secondary electrons at *S*, which multiply in gas by electric field *E* and diffuse along radial distance *r*.

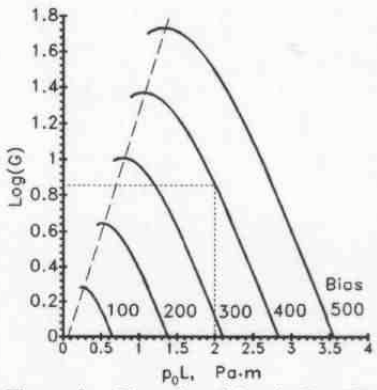

Figure 9. Plot of useful gain *Log(G)* against p_0L for different bias of electrode in volts.

demonstrated with a plate electrode biased at a few hundred volts (V), so that it can operate like a proportional counter (see figure 8). The electron beam strikes the specimen (grounded electrode), and the generated SE are accelerated in the electric field of intensity $E=V/d$. After a short distance, each SE dissipates its acquired energy by colliding with a gas molecule that suffers ionisation or excitation. This process is repeated many times until the SE reaches the detector electrode. As a result, the original SE signal produces an avalanche of gaseous electrons and photons (the products) which can be monitored by methods of particle physics. By this approach, the SE signal is both detected and initially amplified by the gas. When using the ionisation products, the initial *useful* gain G of the device with plane electrodes is given by:

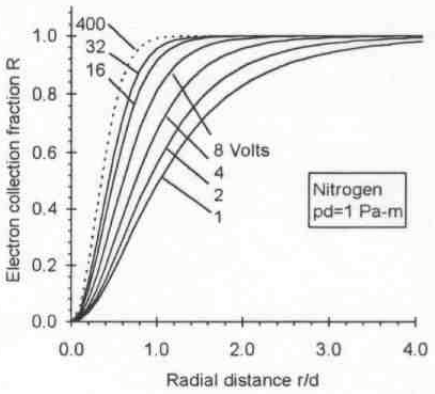

Figure 10. Variation of electron collection fraction R vs. r/d for fixed values of electrode bias (V) at constant $pd=1$ Pa-m.

$$G = \exp\left[p_0 L \left(fAe^{-Bp_0 L/V} - \frac{\sigma_T}{kT} \right) \right] \tag{19}$$

where A and B are constants characteristic of the particular gas and f is a correction constant:

$$f = 1 - \frac{V_m}{V} \tag{20}$$

which accounts for the minimum effective bias V_m required to initiate an avalanche. In the calculation of the useful gain we have taken into account the initial losses of the electron beam given by equation (3). In figure 9, we plot the gain versus the product p_0L for fixed electrode bias, and we note that this function displays a maximum. The condition for operating a GDD with plate electrodes always at the maximum gain has been found to be [17]:

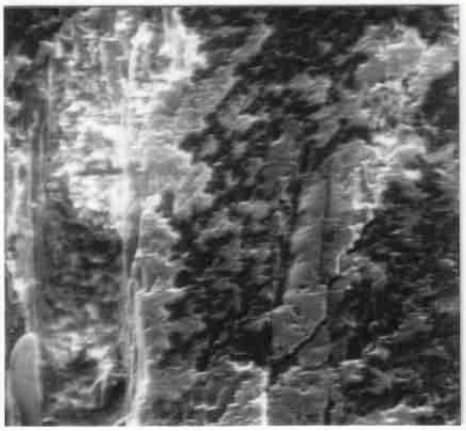

Figure 11. SE image of a Al/Fe rich mineral obtained with GDD, using 10 keV beam, 230 pA, 1.2 mbar of air, field width=290 μm.

$$fAe^{-Bp_0L/V}\left(1-\frac{p_0LB}{V}\right)=\frac{\sigma_T}{kT} \quad \text{(optimum GDD condition)} \qquad (21)$$

For the design and operation of a plate electrode GDD, we need to establish the distribution of SE (and their products) as they travel towards the top electrode. The electrons move in the direction of the anode but they simultaneously diffuse radially on account of their random collisions with the gas. The lateral spread of electrons is governed by a diffusion process, which has been studied by Huxley and Zaazou [23]. Based on this work, we can find the fraction R of SE electrons (multiplied or not) that arrive within a radius r at the detector electrode by:

$$R=1-\left(1-\frac{r^2}{L^2}\right)^{-1/2}\exp\left\{\frac{eV}{2kT\varepsilon}\left[1-\left(1+\frac{r^2}{L^2}\right)^{1/2}\right]\right\} \qquad (20)$$

where ε is the ratio of thermal energy over kinetic energy of electrons. This parameter depends on the applied field, pressure and nature of the gas used, and its availability is critical for the determination of electron distributions. The variation of R versus r/D for fixed values of electrode bias is shown in figure 10. The dotted curve has been drawn by use of an extrapolated value of ε, whilst the rest are based on values tabulated from the literature [12]. The SE signal appears concentrated within a relatively small radius. By choosing the correct size, position and bias of electrode, we can obtain maximum efficiency of detection and best purity of the SE character in an image. An example is given in figure 11 by a SE image showing surface properties of a mineral sample. The same field of view will be compared with an image by the BSE image below. The veracity of signal origin has been shown elsewhere [12,24].

Backscattered electrons

The detection of BSE signal in ESEM can be achieved in a variety of ways. BSE detectors based on scintillating materials, on solid state cells and on gaseous detection have all been used. Because the BSE have high energy, they can pass through the gaseous layer relatively undisturbed before they strike the detector, which can operate in the presence of gas in the usual manner. In fact, the gas creates the benefit of charge dissipation through its ionised state, which is a better alternative than covering the detectors with a conductive layer (aluminium or other). Because the BSE electrons directly strike the uncoated surface of the detector and no signal energy is lost in an added conductive layer, very low energy beam can be used with the highest detection efficiency. Naturally, metallisation of

the detector surface may still be practised for specific detector designs in ESEM. However, both scintillating and solid state materials require an optimised geometry to account for the short working distance generally required. Much work has been done in optimising the shapes of scintillating detectors [25]. An example is shown in figure 13 for a pair of symmetrical detectors, where the shapes are calculated to yield optimum light transmission.

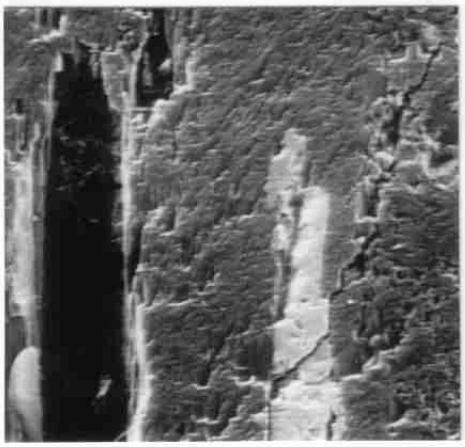

Figure 12. BSE image of same field of view as previous by using the GDD at 4.1 mbar of air with a side electrode wire biased at 10 volts.

An alternative new approach to detect the BSE signal is again with the GDD. This is achieved by detecting the ionisation (or the scintillation) produced by the BSE [24]. The BSE traversing a sufficient distance in the gas produce ionisation (and scintillation) on account of their own energy, which are the primary (i.e. first stage) products of signal-gas interaction. The presence of an external electric field results in further amplification of the signal via the secondary products (i.e. second stage). It is possible to manipulate the detection of various products by various electrode configurations and electrode bias. By such methods, it is also possible to separate the SE from the BSE signal. A simple way, by no means the best, to obtain a BSE image is by using a low bias (e.g. 10 volts) on a wire electrode placed several mm from the side of the specimen at increased gas pressure. Under this condition, the SE do not produce an avalanche amplification while they diffuse to nearby ground surfaces. At the same time, the BSE multiply by creating electron-ion pairs as they traverse their course in the surrounding volume of the wire electrode. The latter detects a current that corresponds to the BSE signal. Figure 12 was made by this method, and its pure BSE nature could be confirmed by comparing it with an image of the same field of view obtained with the scintillating detectors of figure 13.

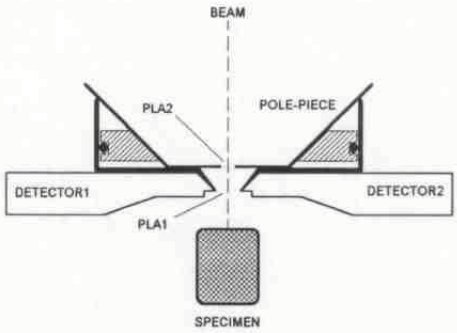

Figure 13. System of scintillating-detector/light-pipes employed in ESEM.

The choice of detector materials, geometry, electronics and multiple detector configurations may be

integrated with the electron optics and gas dynamics requirements of an ESEM to yield best results in future work.

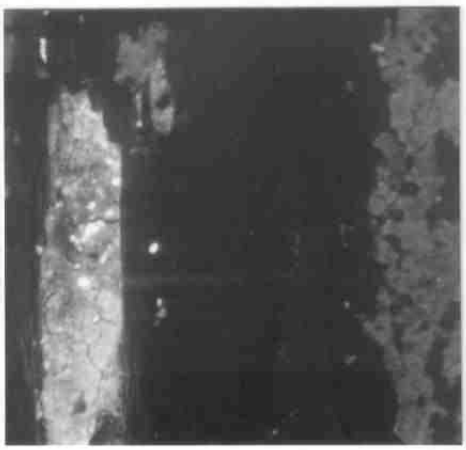

Figure 14. Cathodoluminescence image of same field of view as in figures 11 and 12.

Cathodoluminescence

Cathodoluminescence is the mode of detecting the light generated by the beam-specimen interaction. This is a very powerful method, because the light can be analysed to yield specific information about the specimen. Despite this, it is not widely used for various reasons. One reason is that the vacuum in a SEM limits the range of its applications. For this mode, we require to have the natural surface of a specimen exposed to the beam and not a modified or treated one. ESEM has provided us precisely with this requirement and, hence, this mode has now been freed to cover a limitless number of applications. For the first time, any type of surface can be characterised with this technique, wet or dry, insulating or conducting. Because of the early stage of ESEM developments, CL awaits for its full implementation. Here, we show some early laboratory work. One of the light pipes in figure 13 was cleared of scintillating material and was used as a CL detector. Figure 14 shows the same field of view of the previous mineral specimen, in CL mode. In this image, by proper choice of gas, care was taken to suppress the gaseous scintillation caused by the SE and BSE electrons [21].

The use of CL ancillary equipment, such as spectrophotometers, can make ESEM a most powerful machine for analysis. Furthermore, the same ancillary equipment can be used for separating the light emitted by the beam-specimen interactions from the light emitted by the signal-gas interactions. Those signals can be monitored and analysed, so that not only the CL mode can be practised, but also the power and versatility of the GDD detector operating in its gaseous scintillation mode can be enhanced.

X-rays

The x-ray mode has been incorporated in ESEM. Energy dispersive spectroscopy (EDS) detectors, originally made for a SEM, have been attached to a commercial ESEM by various users and several applications have already been reported.

However, this mode has an inherent difficulty with regard to spatial resolution, because the electron skirt furnishes information from a region much wider than the size of the useful imaging probe. This problem is circumvented in other modes of detection by electronically suppressing the d-c signal level due to background noise, but special attention is required with x-rays.

To recover spatial resolution in EDS analysis, there are, at least, three approaches [11,26]: (a) To operate the ESEM under the lowest possible but sufficient gas pressure to suppress charging artifacts on insulators [27]. Under this condition, the skirt effect may be ignored. (b) To operate the ESEM with a sufficiently short working distance, whereby the skirt decreases its radius to the same order of magnitude as the beam-specimen interaction volume which limits the spatial resolution as in vacuum. (c) To calibrate out (i.e. to subtract) the effects of skirt. The first approach has already been practised without any special modifications. The second approach has some practical difficulties but, nevertheless, it remains a possibility: For example, for a pressure of 500 Pa, 30 keV beam and 10 μm travel distance, we obtain $r_{0.5}=1.4$ μm and $r_{0.9}=9.5$ μm skirt radii for nitrogen by use of equations (15) and (16), respectively. In reality, the nitrogen cross-section might be smaller, or the situation can be improved by using a light gas (e.g. helium), or a higher accelerating voltage of the incident beam, if it is appropriate. The use of a very small aperture (i.e. a few μm) acting both as PLA1 and as a "skirt-mask" close to the specimen, with x-ray detectors placed above the aperture, can restore spatial resolution to the levels of beam-specimen interaction volume (or the aperture size); the known (calibrated under various operating conditions) spectrum due to the aperture material should be subtracted from the total spectrum. With such a small PLA1, very high specimen chamber pressures (up to near atmospheric levels) would also be possible. The latter configuration would constitute a rather dedicated instrument for corresponding applications. However, for general purpose uses, the third approach seems the most promising and comprises various methods: (i) The "difference" of spectra among selected near-by points on the specimen is the most direct one. (ii) The use of a calibrated "skirt-mask", i.e. a very small aperture on top of the specimen is an alternative. (iii) An early attempt has been reported by subtracting an appropriate percentage of an x-ray spectrum of a "raster" from the spectrum of a stationary spot [28]. Another paper deals with the "beam stop" (iv), the "thin foil" (v) and the "pressure variation" (vi) methods [29]. The pressure variation method holds great promise, especially for when accurate experimental data or precise theoretical electron scattering distributions in gas become available. Such tabulated data should take into account the total gas density variation along the beam path in a particular ESEM instrument. Based on such methods, a calibration algorithm can be incorporated in x-ray microanalysis.

Wavelength dispersive spectroscopy (WDS) in ESEM has not been practised yet. However, this mode of detection is both in principle and in practice also possible

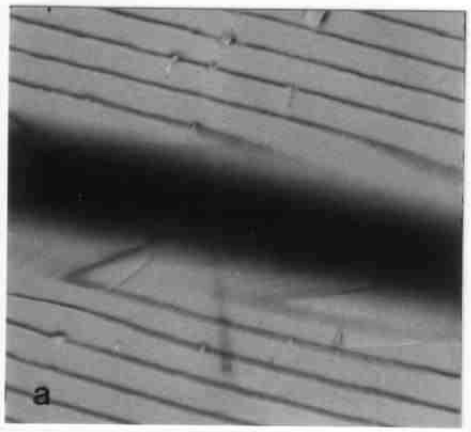

Figure 15. BSE image of diffraction grating (10 μm spacing, gold-coated) with out-of-focus fibre 1.5 mm above the grating, under 15 keV beam, in nitrogen with pressure of (a) 30 Pa and (b) 100 Pa.

to achieve. It is only a matter of time for the manufacturer to adapt the necessary hardware around the ESEM requirements.

BEAM IRRADIATION EFFECTS

It has been shown that ESEM can operate as a routine instrument incorporating all the advantages of a conventional SEM but without the disadvantages of the latter. However, the electron beam irradiation effects still remain a common cause of concern for both instruments, although with some important differences which place ESEM in an advantageous position. Those effects have been studied to various extents in the literature under the topics of charging, contamination, mass loss, heating, electrostatic deformation, hydrolysis, mortality rate, etc.

As mentioned previously, charging is effectively suppressed in ESEM. This can be demonstrated by a sensitive experiment shown in figure 15. The first image shows deformed lines of a gold-coated optical diffraction grating. The deformation is an image artifact caused by the deflection of the electron beam every time it scans near an uncoated wool fibre (shown as an out of focus dark zone) placed 1.5 mm above the focused grating. As soon as we raise the pressure from 30 Pa, in first image, to 100 Pa, in second image, the deformation disappears. The wool fibre no longer charges to a level that would deflect the beam by a visible amount.

Deformation of the specimen itself due to electrostatic forces is also effectively suppressed in ESEM, as are effects due to heating, because charge and heat can be easily dissipated in gaseous and wet environments. Detailed studies for various

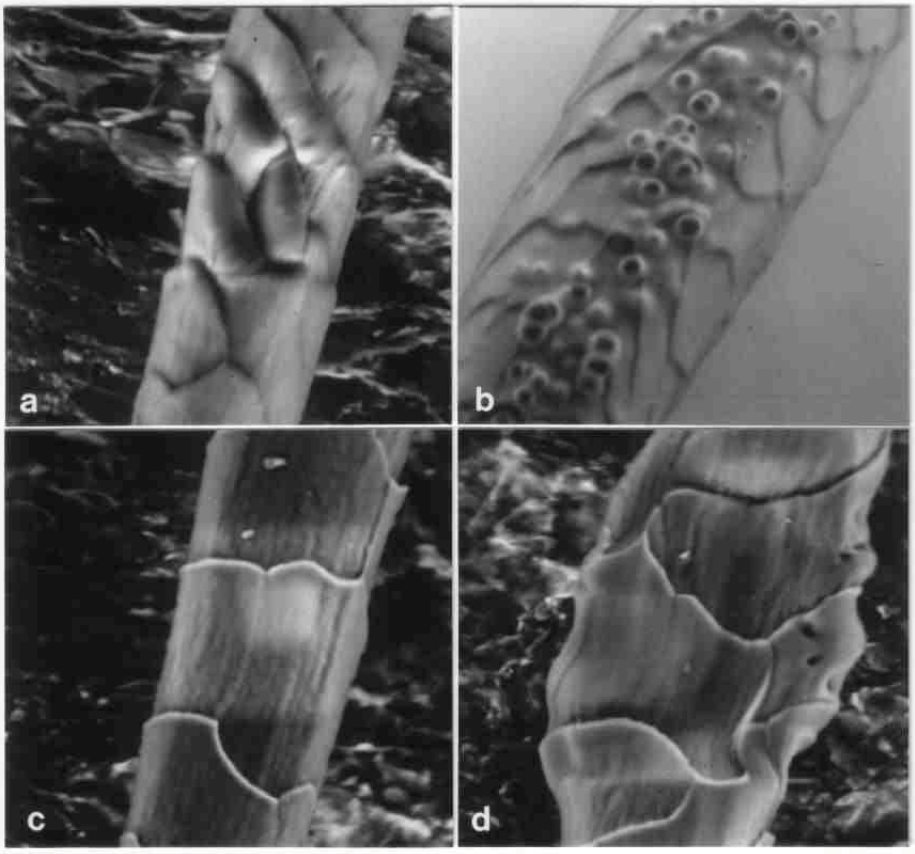

Figure 16. Wool fibres showing irradiation effects after exposure to beam with (a) 15 keV, 850 pA, in argon at 100 Pa, for 5 mins., TV scan rate, (b) 10 keV, 1650 pA, partially immersed in water at room temperature, for 5 mins., (c) 5 keV, 150 pA, in hydrogen at 400 Pa, for 11 mins. (large raster) and 20 mins. (small raster), (d) 20 keV, 430 pA, in hydrogen at 20 Pa, for 4 mins.

classes of applications are now in order to determine the ranges of various parameters under which different beam effects take place, if they do, and to what extent. Some preliminary studies have been initiated in wool research [30,31], and some cases are shown in figure 16. Four different kinds of effect have been caused by deliberately exposing the wool fibre surface to different conditions of beam and gaseous environment. All images in this figure were obtained with BSE scintillating detectors using 5 keV and 150 pA beam following the exposures indicated in the legend. The scanning rate during the irradiation time was 1 frame per second with 250 scanning lines, except for case (a) where the TV scanning rate was used. Perhaps, the most severe effect may be caused by hydrolysis under wet conditions, and the bubbles appearing in (b) may be due to this effect. The white rasters in (c) corresponding to two different magnifications may be due to

simultaneous mass loss and contamination. These are two competing effects and, if properly controlled, they could be used to advantage (although this mechanism is complicated as the two processes may occur at different layers). The swelling deformation in (d) may be due to electrostatic forces under dry conditions at high keV beam. For more details, the reader is referred to the original publications.

Beam effects constitute a very broad topic, and ESEM ideally lends itself for such studies. Conversely, the detailed study and understanding of specimen irradiation is an essential ingredient of ESEM science, especially when ESEM claims the natural surface of objects as its own domain. Beam damage is not new to ESEM and the user should be particularly aware of its possible presence. The best way to control it is by use of a properly designed instrument with the highest sensitivity of detectors, stability and control of beam as well as versatile specimen stages and specimen manipulators. These controls allow for an image to be obtained in the shortest time with minimum irradiation, as it should. Alternatively, new treatment techniques may be devised to render a specimen resistant to damage, such as using scavengers of radicals.

Lastly, beam irradiation has been and can be used to advantage. Some workers have used the patterns, or forms, of beam damage as a means to study the properties of specimens [32]. In another sense, the mechanism that creates "contamination fingers" in electron microscopes can be used with a controlled atmosphere in an ESEM as a means for micro-fabrication.

OPERATION AND APPLICATIONS

The equations governing beam transfer together with the equations governing signal detection define the ranges of various parameters in which ESEM is operable. We may consider the gas pressure as the independent parameter upon which all others depend. Both from experience and theory, we know that pressure can vary from high vacuum up to one atmosphere. For every fixed value of pressure, the range of all other parameters can be determined. For example, the working distance cannot exceed a particular maximum limit and the specimen tilt may be limited. However, both parameters can be extended by choosing a lower value of pressure. In the same way, we can establish the range of accelerating voltage (its minimum value allowable), beam current, gas temperature, etc. Other parameters, such as beam spot diameter, contrast and resolution, specimen stability, etc. depend on the first ones. The most important observation is that ESEM can operate at any pressure level and, hence, SEM is a partial case of it. It is possible to design a *Universal ESEM* that covers the complete pressure range.

Different gases can be used for different applications. If the purpose of gas is only to suppress charging of insulating specimens, practically any gas may be used.

Any relative humidity can be achieved; a dry gas (e.g. nitrogen or argon) can be mixed with and gradually, or abruptly, replaced by water vapour. A water reservoir is usually attached to the specimen chamber to provide a humid environment. Wet specimens can be inserted and maintained in their wet state from ambient conditions by pumping down the specimen chamber to the saturation water vapour pressure. This is achieved by supplying water vapour at the same rate as it is pumped out during pumping down time. Depending on the design of specimen chamber, the specimen insertion can take place within one minute.

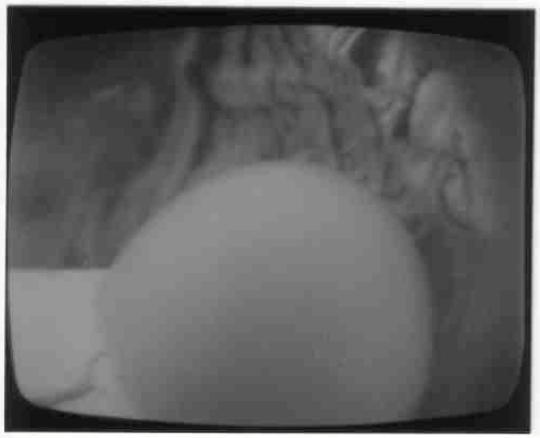

Figure 17. TV frame of water droplet from micro-injector, BSE mode, under 7 keV, horizontal field of view=380 μm.

One of the early applications of ESEM was to study the surface properties of wool fibres by means of observing and measuring the contact angle of water and other liquids (such as detergents), or by observing the water migration in fibre structures, in real time. For such experiments, a micro-injector was designed for the transfer of various liquid chemicals on the specimen [33]. Figure 17 shows

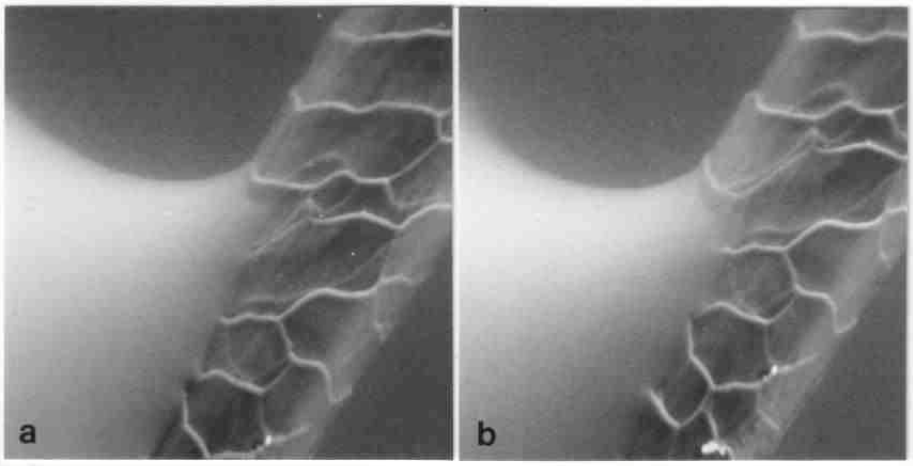

Figure 18. Droplet of water from micro-injector in contact with wool fibre surface at two consecutive locations (a) and (b).

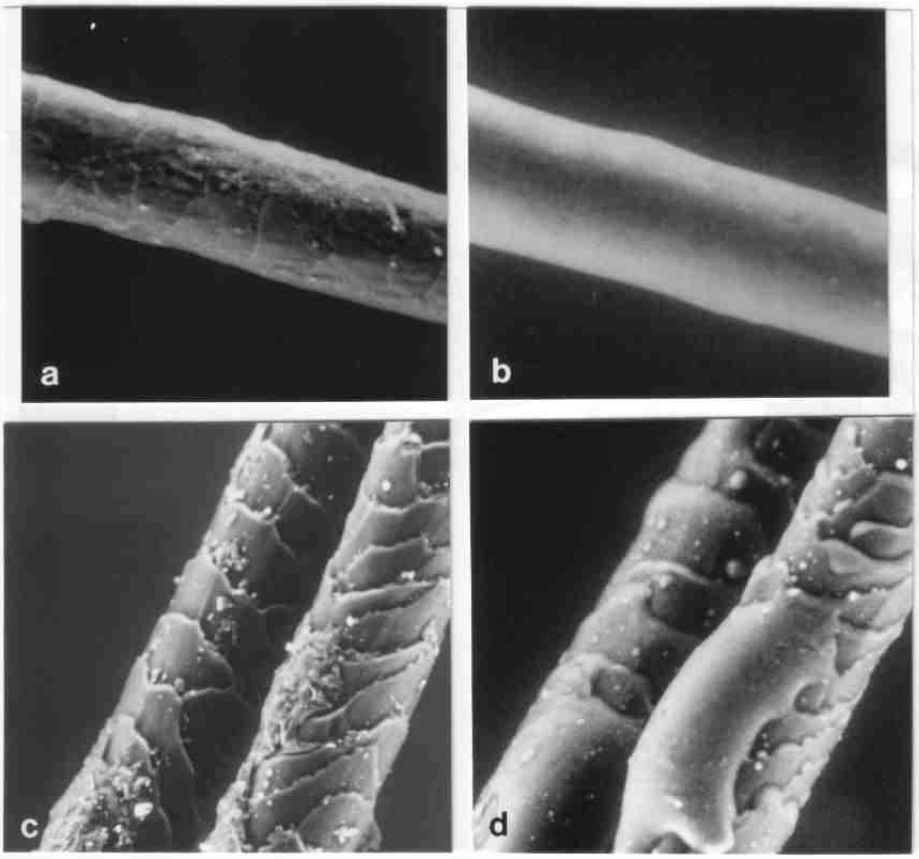

Figure 19. Untreated wool fibres in the dry (a) and wet (b) state. Degreased wool fibres in the dry (c) and wet (d) state showing the differentiation and distribution of suint and dirt particles.

"an instant" of a water droplet at the tip of a glass capillary needle just prior to its absorption by paper tissue in the background. It is a photograph from a single TV frame (1/25 of a second) of a video recording showing "continuous" flow of water. This experiment was performed at room temperature with 7 keV beam. The image was made with an unprocessed BSE signal from the output of a photomultiplier. Figure 18 shows the receding contact angle of water with a clean wool fibre surface in two consecutive positions as the wool fibre is shifted relative to the water droplet; this micrograph was recorded with the usual 50 second scanning time.

Another early application was the study of scouring (cleaning) processes of raw wool contaminated with grease, suint and various particles. Figure 19 shows the difference in the dry (a) and wet (b) state of an untreated wool fibre. A continuous

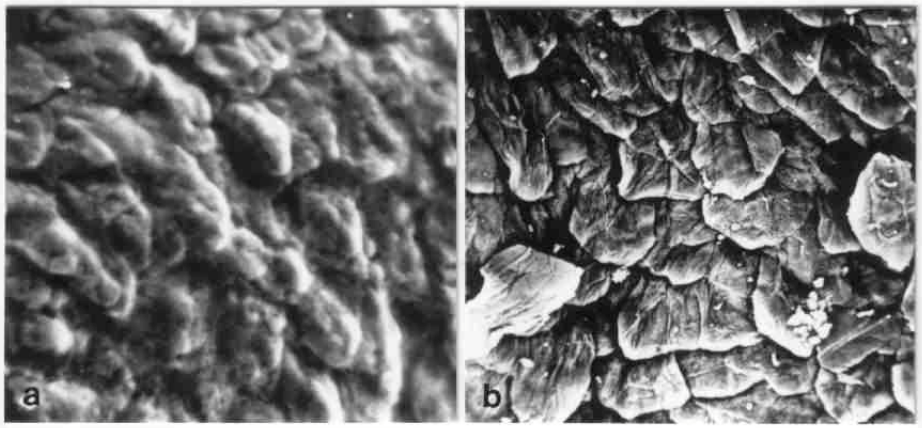

Figure 20. Rat skin (a) untreated, (b) fixed/CPD/gold-coated.

film of aqueous solution of suint covers the fibre and a lump of grease or other low atomic number (Z) contaminant is seen protruding from the liquid surface. Dirt of high Z, of mineral origin, is seen as bright particles. The surface of the suint solution seems to be covered with a scum layer having some holes. When the relative humidity was reduced to near zero, the water evaporated to reveal the uneven thick layer of grease on the fibre. The surface is seen to be mainly of low Z, but with some dirt or suint particles. From the known composition of suint, it is deduced that the scum may be based on calcium and magnesium salts of dicarboxylic acids; this is consistent with the Z-contrast observed. A knowledge of the distribution of suint in raw wool is important in scouring research. Since only the primary follicles produce suint and the water soluble component plays an important role in grease removal, the distribution of suint is of great interest. The fibres can be chemically treated to remove separate fractions of material in a controlled manner, and each time the same specimen can be examined in the ESEM. Thus, after degreasing the wool by extraction with petroleum spirit, the dirt and suint left is seen in figure 19 (c) at low relative humidity. When the humidity was raised to 95%, the location of suint was revealed by its deliquescent nature in (d). Droplets of suint solution were found adhering to every scale along the length of the fibres examined in the sample.

Another application is shown from the biological field. The conventional specimen treatments are useful in revealing certain features. However, the treatments themselves may prove an obstacle, when one is interested in viewing biological components that are invariably removed or altered during specimen treatment. A simple example is given in figure 20 showing an image (a) of fresh rat skin and (b) of fixed/critical-point-dried/gold-coated skin from the same rat. The treated surface shows detail which is masked by a natural layer of biological material in the fresh state. Therefore, various treatments in ESEM may still be

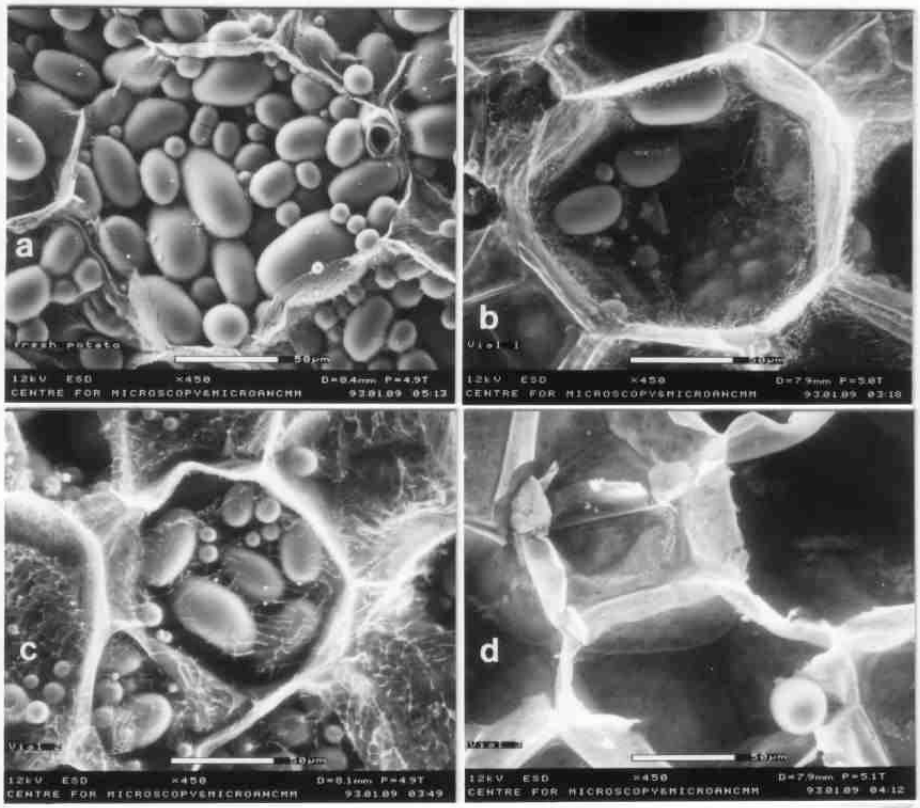

Figure 21. Potato sample: (a) fresh without any treatment, (b) after freeze substitution with gluteraldehyde and 100% methanol, (c) after freeze substitution with 100% methanol, (d) after chemical fixation with gluteraldehyde, osmium and critical point dried. (Reprinted by permission of authors and Wiley-Liss, Inc., a subsidiary of John Wiley & Sons, Inc., from article in "Effects of four different processing techniques on the microstructure of potatoes: Comparison with fresh samples in the ESEM" by Uwins PJR, Murray M and Gould RJ, Microsc. Res. Technique 1993;25:412-418).

used for the purpose of revealing additional information. Other effects of specimen treatments are described below.

All application images shown up to this point were obtained in the BSE mode by the experimental ESEM prototype without any image processing. In the remaining examples, the images were obtained in the secondary electron mode by the use of the GDD in a commercial ESEM, which has been primarily based on this mode of detection. It is envisaged that all other modes of detection will be fully utilised as soon as they become fully available on the commercial instrument.

Various conventional specimen treatments in SEM may mask particular information, or may produce serious artifacts. Uwins et al. [34] have studied the

effects of four different processing techniques on the microstructure of potatoes by comparison with fresh samples in the ESEM. Figure 21 shows some of the treatment effects. Micrograph (a) shows a fresh sample dissected from a potato and examined immediately in the ESEM. The polygonal cell outline, tightly packed starch grains and the smooth or faintly wrinkled surface cell indicate a practically undisturbed specimen. Micrograph (b) shows that the treatment has removed a considerable number of starch granules and an irregular network of material shows along the cell margins. Image (c) also shows significant but somehow less distortion with a wrinkled surface texture. Image (d) shows nearly all the starch grains gone but with better polygonal cell outline and roughened walls. All those and other treatments and conditions have invariably showed various artifacts.

The examination of botanical specimens in ESEM is an easy and straight forward field of application, and many workers have taken advantage of it. For example, recently, Gribble et al. [35] have looked at the surface of normal and vitrified leaves of *Gypsophila paniculata* (Babies Breath) cultured in vitro. Wallace et al. [36] have investigated the pollen-stigma interactions in *Macadamia* and *Grevillea*. Water is a limiting resource during fertilisation in higher plants and surface secretions are lost after conventional fixation for SEM. Monitoring adhesion and germination using ESEM provides a unique means of studying these recognition events in flowering plants. Figure 22 shows images of pollen from the commercial *Macadamia integrifolia* without any preparation. In micrograph (a), we see hydrated triculpate pollen collected from the pistil after anthesis showing potential sites of pollen tube emergence at pollen grain extremities. Micrograph (b) shows germinated grain with tube having emerged and grown the stigma surface. In micrograph (c), we see a site of pollen tube emergence showing the transition from the textured surface of the pollen exine layer to the base of the pollen tube.

With ESEM we can see things not possible to see with other microscopes. O'Brien et al. [37] have used ESEM to study quantitative and qualitative differences in microbial populations between different mungbean seeds. The outer texture layer of seeds is easily removed or damaged following standard processing protocols for conventional SEM. Various regions of different seeds have been compared with both techniques, and magnifications of different bacteria up to 48000× have been presented. In their studies of micro-organisms in ESEM, Collins et al. [38] have demonstrated some unique advantages of ESEM such as the revealing of sub-surface structures of uncoated specimens.

Various ancillary devices can be constructed to suit different applications. Extensometers and other specimen deformation equipment can be attached to an ESEM to take advantage of the fact that a deforming surface can be monitored without the need of conductive coatings [30]. The possibility of examining the

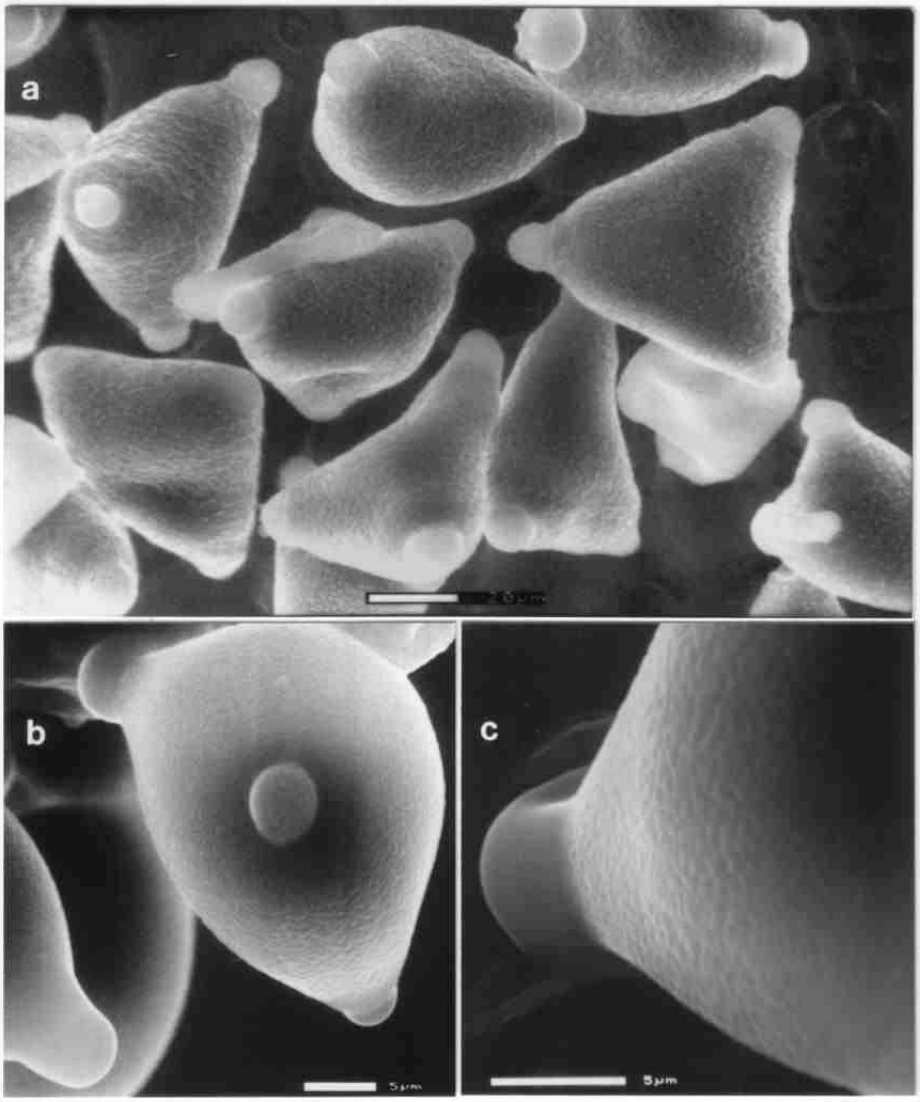

Figure 22. Pollen from *Macadamia integrifolia* Maiden and Betche: (a) Hydrated triculpate pollen, scale bar=20 μm. (b) Germinated pollen grain with tube, bar=5 μm. (c) Site of pollen tube emergence, bar=5 μm. (Courtesy of Wallace HM, Uwins PJR and McConchie CA).

natural surface of specimens allows the variation of temperature over the widest range. Cold and hot stages have been built to allow the continuous variation and observation of surface properties in-situ. For the micro-electronics research and applications, dedicated specimen chambers have been built around the ESEM principle [39]. Fast testing and measurement of line-widths and other micro-

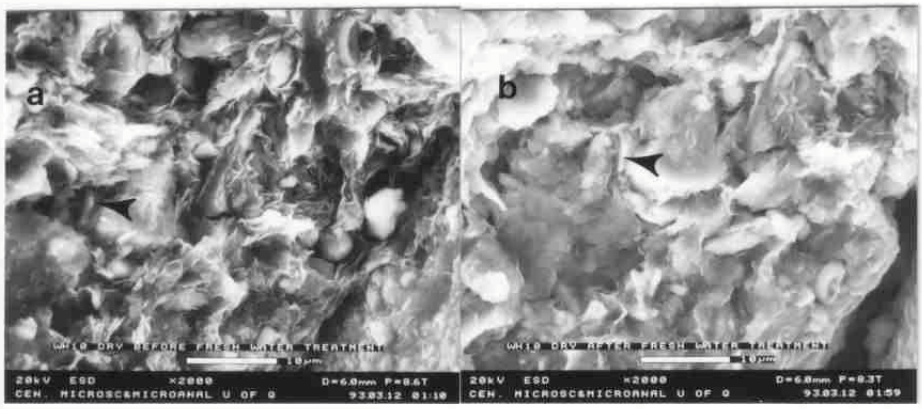

Figure 23. (a) Smectite in mudrocks from fresh outcrop before freshwater injection, (b) dry after freshwater injection, scale bar =10 μm. (Reprinted with kind permission from the authors and Elsevier Science-NL, Sara Burgerhartstraat 25, 1055 KV Amsterdam, The Netherlands, from article in "Observation of water-clay reactions in water-sensitive sandstone and mudrocks using an environmental scanning electron microscope" by Huggett JM and Uwins PJR, J. Petroleum Science and Engineering 10:211-222, 1994).

electronics structures are now a reality. Micro-fabrication can be practised by controlling the gaseous composition and beam parameters [40,41].

Surface chemistry and chemical reactions in general are now open to new possibilities with ESEM. Corrosion studies of stainless steel where various products are formed can be monitored and analysed in-situ, before, during and after formation [42]. Morphology of nitric acid and water ice films have been examined to simulate stratospheric cloud surfaces in order to obtain laboratory data on solubilities and heterogeneous reaction rates [43]. Crystal and plaque formation associated with bio-corrosion has been studied through imaging and microanalysis [44]. Surface properties of various materials can be studied by observing the wetting properties and differential hygroscopicity on a microscale [45]. Ink on paper can be easily seen since the secondary electron imaging mode is sensitive to, and allows, the differentiation of surface layers [46].

In petroleum science and engineering, several studies of water/clay reactions in water sensitive sandstone and mudrocks have been done [47,48]. Different fluids (e.g. freshwater, or KCL-based drilling mud) can be used in the tests and the same area can be viewed before and after treatment. By examining the extent to which illite-smectite and smectite swell, when treated with water, it has been possible to access the importance of clay swelling as a drilling problem in these rocks. For example, figure 23 shows such an effect. Smectite in mudrocks obtained from fresh outcrop shows the clay swollen and expanded to fill the pore on the right-hand side; to facilitate identification, a marker shows the same point on the specimen surface before and after treatment.

Electron dispersive spectroscopy and microanalysis in ESEM has demonstrated new uses and great promise [49,50]. It should not be long before the x-ray mode is used routinely in all fields of application.

CONCLUSION

It has been shown that ESEM is an established instrument, method and technique for in-situ studies in unlimited ways. It has become the first in-situ commercially available electron microscope, not just an accessory to existing instruments. As a result, this method and technique have become available to a large number of workers, and a voluminous literature has already emerged.

With an ESEM, we can examine practically any surface in-situ. Wet specimens can retain their natural state because a 100% relative humidity can be maintained routinely. Dry specimens can also be examined regardless of their electrical conductivity. The environmental gas becomes a good conductor because of the ionising radiation present and, thus, it substitutes the conventional conductive coatings or other treatments used to prevent specimen charging.

The imaging power and information collection capability of an ESEM is not compromised over that of a conventional SEM. Detection of secondary electron, backscattered electron, cathodoluminescence and x-rays have been practised. In particular, a novel detection method has been introduced, namely, the use of the gas itself as a detection medium. The secondary and backscattered electrons interact with the gas and produce gaseous ionisation and scintillation. The products of signal-gas interaction can be monitored with suitable means to form corresponding images. One particular form of the gaseous detection device has been used for the secondary electron image and it has become the basic imaging mode of the first manufactured ESEM.

The scope of ESEM has been and can be further expanded by the introduction of ancillary equipment to handle, or manipulate the specimens in-situ, such as:

(a) Temperature controls (hot and cold stages).
(b) Deformation devices for extension, fatigue, vibration, abrasion, etc..
(c) Micro-injectors for liquid deposition and chemical reactions.
(d) Computerised specimen positioning (specimen stages) for finding features and repositioning specimen in the same field of view before and after treatment.
(e) Computerised control of gaseous environment.
(f) New preparation techniques to control or intentionally expose particular features of the natural surface under examination.
(g) New preparation techniques to control or reduce irradiation effects on sensitive specimens.

(h) Special action devices, such as laser beam, molecular beam, ion beam, electron beam, electrical or magnetic micro-devices and others.

For optimum results, all above applications and ancillaries presuppose a basic, or core, ESEM electron optics column capable of transferring an electron beam in a gaseous environment with minimum electron losses. This column must be integrated with efficient detection means. The basic requirements have been successfully fulfilled in practice, and theory has shown that significant improvements can be expected in the future.

ACKNOWLEDGEMENTS

I wish to thank Professor PL Gai for inviting me to contribute this chapter. I am grateful to Dr. Philippa JR Uwins for providing me with prints for figures 21, 22 and 23 and with permission to reproduce them from published works of hers and her co-workers; specifically to Drs. HM Wallace and CA McConchie for allowing the unpublished micrographs and comments of figure 22.

REFERENCES

1 Ardenne M. Das Elektronen-Rastermikroskop. Theoretische Grundlagen. Zeits. Physik 1938;109:553-572.
2 Ardenne M. Das Elektronen-Rastermikroskop. Praktische Ausfürung. Zeits. Techn. Physik 1938;19:407-416.
3 Ardenne M. Über die Möglichkeit der Untersuchung lebender Substanz mit Elektronenmikroskopen. Zeits. Techn. Physik 1939;20:239-242.
4 Ardenne M and Friedrich-Freksa H. Die Auskeimung der Sporen von Bacillus vulgatus nach vorheriger Abbildung im 200-kV-Universal-Elektronenmikroskop. Naturwiss. 1941;29:523-528.
5 Ardenne M. Reaktionskammer-Übermikroskopie mit dem Universal-Elekrtonenmikroskop. Zeits. Phys. Chemie, Abteilung B. 1942;B52:61-71.
6 Stoyanova IG, Nekrasova TA and Biriusova BI. Research on the action of radiation on bacteria in the wet microchamber of the electron microscope. Akad. Nauk. SSR Doklady 1960;131:195-198.
7 Stoyanova IG. Use of gas microcells in electron microscopy. Akad. Nauk. SSR Izvestiya, ser. Fisicheskaya 1961;25:715-721.
8 Dupouy G, Perrier F and Durrieu L. Microscopie électronique.-L'observation des objets en milieu gazeux. Application à l'étude de la contamination dans le microscope électronique. Compt. Rend. 1962;254:3786-3791.
9 Parsons DF, Matricardi VR, Moretz RC and Turner JN. Electron microscopy and diffraction of wet unstained and unfixed biological objects. Adv. Biol. Med. Phys. 1974;15:161-271.
10 Butler EP and Hale KF. Dynamic Experiments in the Electron Microscope. Practical Methods in Electron Microscopy. North-Holland Publishing Company, Amsterdam; 1981;9.
11 Danilatos GD. Foundations of Environmental Scanning Electron Microscopy. Adv. Electronics and Electron Phys. 1988;71:109-250.
12 Danilatos GD. Theory of the Gaseous Detector Device in the ESEM. Adv. Electronics and Electron Phys. 1990;78:1-102.
13 Danilatos GD. Bibliography of environmental scanning electron microscopy. Microsc. Res. Technique 1993;25:529-534.

14 Danilatos GD. Gas flow properties in the environmental SEM. Microbeam Analysis-1991 (Ed. DG Howitt), San Francisco Press, San Francisco 1991;201-203.
15 Bird GA. Monte Carlo simulation of gas flows. Ann. Rev. Fluid Mech 1978;10:11-31.
16 Jost K and Kessler J. Die ortsverteilung mittelschneller elektronen bei mehrfachstreuung. Zeits. Phys. 1963;176:126-142.
17 Danilatos GD. Equations of charge distribution in the environmental scanning electron microscope (ESEM). Scanning Microscopy 1990;4:799-823.
18 Wells, Oliver C. Scanning Electron Microscopy. McGraw-Hill Book Company, New York, 1974;20-36.
19 Danilatos GD. Environmental scanning electron microscope: Some critical issues. Scanning Microscopy 1993; Supplement 7:57-80.
20 Danilatos GD. A gaseous detector device for an environmental SEM. Micron and Microscopica Acta 1983;14:307-319.
21 Danilatos GD. Cathodoluminescence and gaseous scintillation in the environmental SEM. Scanning 1986;8:279-284.
22 Danilatos GD. Secondary-electron imaging by scintillating gaseous detection device. Proc. 50th Annual Meeting EMSA (Ed. GW Bailey, J Bentley and JA Small), San Francisco Press, San Franciso 1992;1302-1303.
23 Huxley AG and Zaazou AA. Experimental and theoretical studies of slow electrons in air. Proc. Roy. Soc. Lond. 1949;196:402-426.
24 Danilatos GD. Mechanisms of detection and imaging in the ESEM. J. Microsc. 1990;160:9-19.
25 Danilatos GD. Design and construction of an atmospheric or environmental SEM (Part 3). Scanning 1985;7:26-42.
26 Danilatos GD. Environmental scanning electron microscopy and microanalysis. Mikrochim. Acta 1994;114/115:143-155.
27 Robinson VNE and Robinson BW. Materials characterisation in a scanning electron microscope environmental cell. Scanning Electron Microscopy (SEM Inc. AMF O'Hare) 1978;I:595-602.
28 Bolon RB. X-ray microanalysis in the ESEM. Microbeam Analysis-1991, (Ed. D.G. Howitt) San Francisco Press, San Francisco, 1991;199-200.
29 Bilde-Soerensen JB and Appel CC. Energy-dispersive x-ray spectrometry in the environmental scanning electron microscope. Proc. 48th Annual Meeting Scandinavian Soc. El. Microsc., Aarus, Denmark, 1996;4-5.
30 Danilatos GD and Brooks JH. Environmental SEM in wool research - present state of the art. Proc. 7th Int. Wool Textile Research Conference, Tokyo, 1985;I:263-272.
31 Danilatos GD. Beam-radiation effects on wool in the ESEM. Proc. 44th Annual Meeting EMSA 1986;674-675.
32 Heavens JW, Keller A, Pope JM and Rowell DM. Beam induced changes in the scanning electron microscopy of poly(oxymethylene). J. Mat. Sci. 1979;5:53-62.
33 Danilatos GD and Brancik JV. Observation of liquid transport in the ESEM. Proc. 44th Annual Meeting EMSA 1986;678-679.
34 Uwins PJR, Murray M and Gould RJ. Effects of four different processing techniques on the microstructure of potatoes: Comparison with fresh samples in the ESEM. Microsc. Res. Technique 1993;25:412-418.
35 Gribble K, Sarafis V, Nailon J, Holford P and Uwins P. Environmental scanning electron microscopy of the surface of normal and vitrified leaves of *Gypsophila paniculata* (Babies Breath) cultured in vitro. Plant Cell Reports 1996;15:771-776.
36 Wallace HM, Uwins PJR and McConchie CA. Investigation of pollen-stigma interactions in *Macadamia* and *Grevillea* using ESEM. J. of Computer-Assisted Microscopy 1992;4:231-234.
37 O'Brien GP, Webb R.I, Uwins PJR, Desmarchelier PM and Imrie BC. Suitability of the environmental scanning electron microscope for studies of bacteria on mungbean seeds. J. of Computer-Assisted Microscopy 1992;4:225-229.
38 Collins SP, Pope RK, Scheetz RW, Ray RI, Wagner PA and Little BJ. Advantages of environmental scanning electron microscopy in studies of micro-organisms. Microsc. Res. Technique 1993;25:398-405.

39 Yamaguchi T, Kawata S, Suzuki S, Sato T and Sato Y. New linewidth measurement system using environmental scanning electron microscope technology. Proc. Intern. Microprocess Conf. Jpn. J. Appl. Phys. 1993;32 (Part 1, No. 12B):6277-6280.
40 Danilatos GD. Environmental scanning electron microscope: A new tool for inspection and testing. Digest of Papers, MicroProcess '93, 6th Intern. MicroProcess Conf. 1993;B-3-1:102-103.
41 Charyshkin E, Kinaev NN, Waterworth M, Cousens DR, Calos N, Bostrom T and Ilyushechkin A. In-situ electron microscopy studies of hot filament chemical vapour deposition diamond thin film growth in an environmental SEM. Phys. Stat. Sol. (a) 1996;154:43-54.
42 Gerristead WR, Link LF, Paciej RC, Damiani P and Li H. Environmental scanning electron microscopy for dynamic corrosion studies of stainless steel piping used in UHP gas distribution systems. Microsc. Res. Technique 1993;25:523-528.
43 Keyser LF and Leu Ming-Taun. Morphology of nitric acid and water ice films. Microscopy Res. Technique 1993;25:434-438.
44 Geiger SL, Ross TJ and Barton LL. Environmental scanning electron microscope (ESEM) evaluation of crystal and plaque formation associated with biocorrosion. Microsc. Res. Technique 1993;25:429-433.
45 Parra R. A method to detect variations in the wetting properties of microporous polymer membranes. Microsc. Res. Technique 1993;25:362-373.
46 Rask JH, Flood JE, Borchardt JK and York GA. The ESEM used to image crystalline structures of polymers and to image ink on paper. Microsc. Res. Technique 1993;25:384-392.
47 Baker JC, Uwins PJR and Mackinnon IDR. ESEM study of authigenic chlorite acid sensitivity in sandstone reservoirs. J. Petroleum Science and Engineering 1993;8:269-277.
48 Huggett JM and Uwins PJR. Observation of water-clay reactions in water-sensitive sandstone and mudrocks using an environmental scanning electron microscope. J. Petroleum Science and Engineering 1994;10:211-222.
49 Bolon RB, Robertson CD and Lifshin E. The environmental SEM: A new way to look at insulators. Microbeam Analysis-1989, (Ed. PE Russell) San Francisco Press, San Francisco, 1989;449-452.
50 Egerton-Warburton LM, Griffin BJ and Kuo J. Microanalytical studies of metal localisation in biological tissues by environmental SEM. Microsc. Res. Technique, 1993;25:406-411.